HDI-Former: Hybrid Dynamic Interaction ANN-SNN Transformer for Object Detection Using Frames and Events

Dianze Li^{1,2} Jianing Li¹ Xu Liu^{3,2} Zhaokun Zhou^{2,1} Xiaopeng Fan^{3,2} Yonghong Tian^{1,2}

¹ Peking University ² Peng Cheng Laboratory

³ Harbin Institute of Technology

Abstract

Combining the complementary benefits of frames and events has been widely used for object detection in challenging scenarios. However, most object detection methods use two independent Artificial Neural Network (ANN) branches, limiting cross-modality information interaction across the two visual streams and encountering challenges in extracting temporal cues from event streams with low power consumption. To address these challenges, we propose HDI-Former, a Hybrid Dynamic Interaction ANN-SNN Transformer, marking the first trial to design a directly trained hybrid ANN-SNN architecture for high-accuracy and energyefficient object detection using frames and events. Technically, we first present a novel semantic-enhanced selfattention mechanism that strengthens the correlation between image encoding tokens within the ANN Transformer branch for better performance. Then, we design a Spiking Swin Transformer branch to model temporal cues from event streams with low power consumption. Finally, we propose a bio-inspired dynamic interaction mechanism between ANN and SNN sub-networks for cross-modality information interaction. The results demonstrate that our HDI-Former outperforms eleven state-of-the-art methods and our four baselines by a large margin. Our SNN branch also shows comparable performance to the ANN with the same architecture while consuming 10.57× less energy on the DSEC-Detection dataset. Our open-source code is available in the supplementary material.

1. Introduction

DAVIS cameras [4, 20, 32, 53], namely hybrid vision sensors, combine a bio-inspired event camera and a conventional frame-based camera within the same pixel array to complement each other. Event cameras [15], with their high temporal resolution, dynamic range, and low power consumption, detect light changes through dynamic events to overcome conventional camera limitations in high-speed

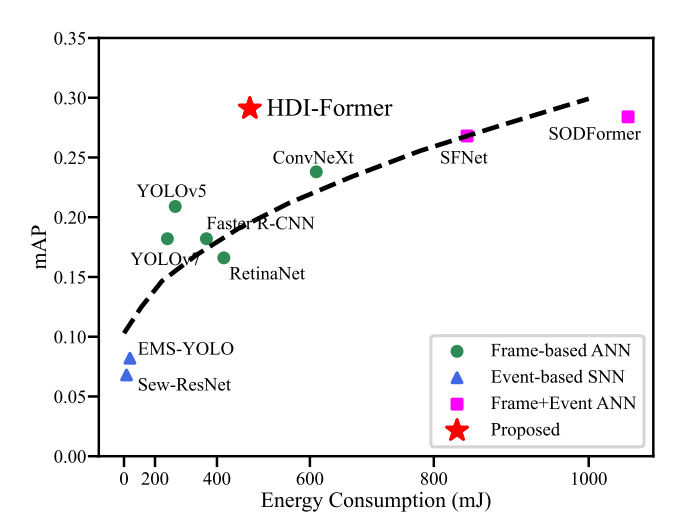


Figure 1. Comparison of our HDI-Former with state-of-theart methods on the DSEC-Detection dataset. Our HDI-Former achieves a significant mAP improvement over unimodal methods while keeping comparable energy consumption, and it outperforms multimodal methods while reducing energy consumption.

motion blur and challenging lighting conditions. Conversely, frame-based cameras capture absolute brightness with fine textures, addressing event camera shortcomings in static or texture-less scenarios. A trend is emerging in leveraging the complementary advantages of frames and events for various computer vision tasks [18, 35]. Nevertheless, how to design a high-accuracy and energy-efficient object detection model for two heterogeneous visual streams remains a challenging problem.

Most multimodal object detectors rely on two separate branches of Artificial Neural Networks (ANNs) [5, 6, 8, 26, 27, 35, 36, 39, 46, 50, 51, 66, 77], limiting the cross-modality interaction between two visual streams and resulting in high energy consumption. More specifically, most existing methods typically convert asynchronous events into an image-like representation [17, 67] and then directly input them into the ANN detection backbone (e.g., SSD [47] and YOLO [60]). However, Convolutional Neural Networks (CNNs) have limited global spatial modeling capa-

bilities, resulting in lower performance compared to Transformers [29], and processing event streams with ANNs involves high computational complexity and energy consumption. Additionally, two separate ANN branches process images and events individually and then generate the final result using a fusion module [5, 35, 46] in this detection paradigm. Nevertheless, processing two visual streams independently ignores cross-modality information interaction which is crucial for the complementary utilization of fine texture frames and dynamic events. In fact, the biological visual system processes fine texture and dynamic sensing in a more interconnected manner than previously thought [28, 64]. Yet, there is no work to design a dynamic interaction neural network with lower power consumption specifically for object detection.

Spiking Neural Networks (SNNs) [11, 41, 62, 78] excel in capturing temporal dynamics for event-based vision with low power consumption, but they are rarely used for multimodal object detection tasks. In general, SNNs utilize binary spikes for neural communication, potentially enabling energy-efficient computation [21, 52]. Most SNN object detectors [7, 24, 30, 40] directly convert ANNs to SNNs, relying on large timesteps and the performance of the original ANN. Recent advancements [3, 9, 14, 65, 72] using surrogate gradients [54] allow for direct training of SNNs, achieving energy-efficient object detection with fewer timesteps. Nonetheless, these single-modality SNNs, processing only event streams, may be hard to achieve highaccuracy detection. A promising method [73] is to design hybrid neural networks by combining ANNs and SNNs to leverage the strengths of both. Although some hybrid neural networks [2, 71] integrate ANNs and SNNs to process two heterogeneous visual streams, they are not explicitly designed for object detection. Furthermore, their subnetworks operate independently and are not directly trained, which may hinder them from fully leveraging the complementary benefits of frames and events.

To address the aforementioned problems, we propose a Hybrid Dynamic Interaction ANN-SNN Transformer, namely HDI-Former, which is the first to directly train a hybrid ANN-SNN architecture for high-accuracy and energyefficient object detection using frames and events. Indeed, this work does not optimize two independent CNN-based branches. In contrast, it seeks to overcome the following challenges: (i) How can we design a novel attention mechanism to achieve high accuracy in the ANN Transformer branch? (ii) How do we create an energy-efficient SNN Transformer branch for event-based object detection? (iii) What is the interaction mechanism for hybrid ANN-SNN branches that benefits two streams? To this end, we first present a novel semantic-enhanced self-attention mechanism to enhance the correlation between image encoding tokens within the ANN Transformer branch. Then, we design an energy-efficient Spiking Swin Transformer branch to use rich temporal cues from event streams. Finally, we introduce a bio-inspired dynamic interaction mechanism between ANN and SNN sub-networks to achieve cross-modality interaction. The results show that our HDI-Former outperforms the state-of-the-art methods by a large margin and our SNN branch achieves comparable performance to the corresponding ANN with less energy consumption. As shown in Fig. 1, our HDI-Former reaches the best balance between performance and energy consumption. The main contributions of this paper are summarized as follows:

- We propose a directly trained Hybrid Dynamic Interaction ANN-SNN Transformer (i.e., HDI-Former), which achieves high-accuracy and energy-efficient object detection using frames and events.
- We present a novel semantic-enhanced self-attention in the ANN branch to enhance the correlation between image encoding tokens for better detection performance.
- We design an energy-efficient Spiking Swin Transformer branch that achieves the best performance in directly-trained SNNs for event-based data while matching ANN performance with 0.1× energy consumption.
- We introduce a bio-inspired dynamic interaction mechanism between ANN and SNN sub-networks to enhance cross-modality information interaction for leveraging the complementarity of frames and events.

2. Related Work

Neuromorphic Object Detection. The existing object detectors [23, 35] utilizing event cameras can be broadly classified into two categories. The first category [25, 37, 56, 59, 69, 80] involves single-modality approaches that solely process the event stream. These methods typically convert events into 2D image-like representations, which are then fed into feed-forward CNN-based backbones [25, 69, 80] or RNN-based object detectors [37, 56, 59]. While these ANNs exhibit high performance, they also come with high computational complexity and energy consumption. More recently, there has been exploration into energyefficient SNN-based object detectors, including ANN-to-SNN conversion models [7, 24, 30, 40] and directly trained SNNs [3, 9, 14, 65, 72]. However, it's evident that relying solely on dynamic event streams may not achieve satisfactory performance in static or slow-motion scenarios that require precise detection of static fine textures. The second category comprises multimodal approaches that combine frames and events. Existing multimodal object detectors [26, 27, 35, 36, 51] utilize two independent CNN branches to handle each visual stream and then predict joint detection results using post-processing or end-to-end aggregation fusion modules. However, one drawback is that the limited spatial modeling ability of these CNN models results in a significant performance gap compared to main-

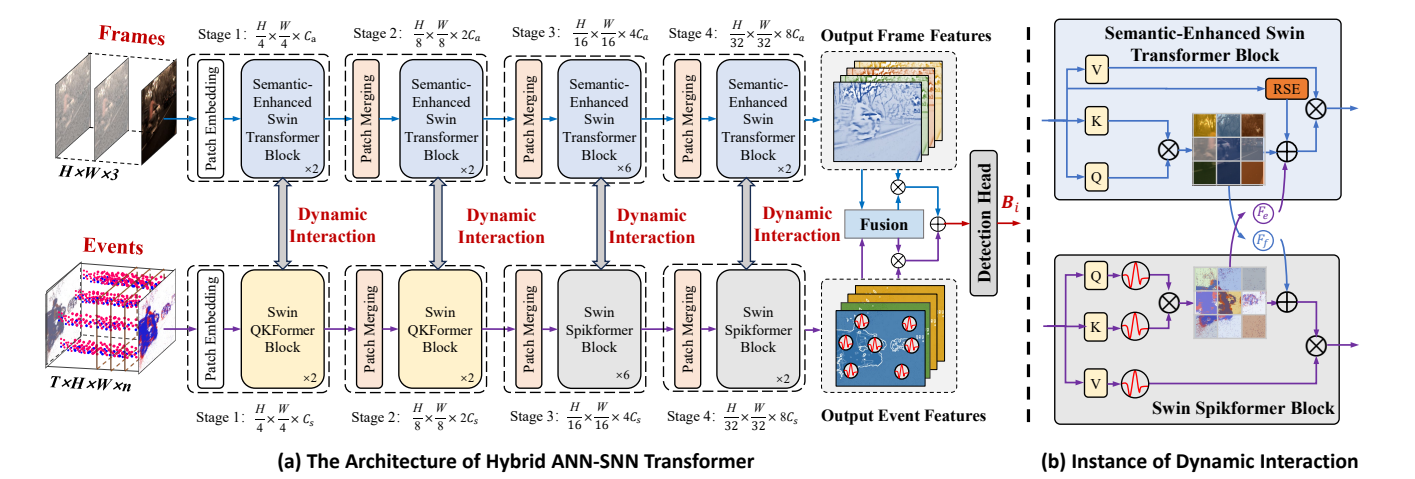


Figure 2. The pipeline of Hybrid Dynamic Interaction ANN-SNN Transformer (HDI-Former). (a) Our HDI-Former consists of two sub-networks and connects an ANN and an SNN via dynamic interaction. The ANN branch processes frames using Semantic-Enhanced Swin Transformer blocks, while the SNN branch handles events with Swin QKFormer and Swin Spikformer blocks. Finally, an asynchronous fusion module [35] combines two streams to predict the detection results. (b) A bio-inspired Dynamic Interaction mechanism between ANN and SNN sub-networks to achieve cross-modality interaction and leverage the complementarity of two streams.

stream Transformer models [19, 57]. Another issue is that two independent ANN branches processing heterogeneous visual streams in the same manner would neglect cross-modality interaction, leading to incomplete utilization of the complementary attributes from frames and events. Thus, this work aims to design a hybrid Transformer with low power consumption to fully leverage the complementarity of two heterogeneous visual streams.

Hybrid Neural Networks. Hybrid neural networks [73] aim to achieve both high accuracy and energy efficiency by combining the strengths of ANNs and SNNs. Due to the development of hybrid vision sensors [4, 20, 32, 53] and neuromorphic computing hardware, there is a growing trend to design hybrid neural networks. In one class of methods [1, 33, 34, 44], SNNs are employed for efficient encoding and feature extraction of spatiotemporal events, followed by different ANN backbones for various visual tasks. However, these single-modality hybrid neural networks are only suitable for processing mere event streams. Another type of methods [2, 71, 73] adopts two branches of ANNs and SNNs to process multimodal frame and event streams simultaneously. The ANN is tasked with extracting features from the frames while the SNN processes events directly. For example, Aydin et al. [2] design an energyefficient hybrid ANN-SNN architecture for human pose estimation. Zhao et al. [73] propose the general design and computation of hybrid neural networks by hybrid units for object tracking. Nevertheless, these hybrid models have not explored the object detection task. Meanwhile, the backbones of their two branches are usually independent of each other, making it difficult for them to interact with each other. Therefore, we propose a dynamic interaction hybrid ANN-SNN model to process two heterogeneous visual streams.

3. Method

3.1. Dynamic Interaction ANN-SNN Framework

This work aims to design a directly-trained Hybrid Dynamic Interaction ANN-SNN Transformer (HDI-Former), which makes complementary use of frames and events to maximize object detection performance. As shown in Fig. 2, our HDI-Former consists of three novel modules: Semantic-Enhanced Swin Transformer for processing RGB frames (ANN), Spiking Swin Transformer for modeling event streams (SNN), and Dynamic Interaction between them. More precisely, we adopt the Swin Transformer [48] as the backbone since it achieves state-of-the-art performance among Transformer architectures. We then enhance the correlation of tokens by involving relative semantic information to further extract fine-grained spatial features from RGB frames. Then, we present a Spiking Swin Transformer to leverage the rich temporal cues from the continuous event stream. Meanwhile, a bio-inspired dynamic interaction between ANN and SNN sub-networks is designed to facilitate cross-modality information interaction. Finally, an asynchronous fusion module [35] is utilized to combine two visual flow features complementarily, feeding them into the detection head to predict the final results.

Aiming to implement cross-modality interaction for better utilization of the complementarity of frames and events, we propose a bio-inspired dynamic interaction mechanism between ANN and SNN sub-networks as motivated by the biological vision system in perceiving dynamic and fine textures [55, 64]. Specifically, this operation makes complementary use of the two modalities and integrates spatiotemporal representations by referencing each other's attention maps. To illustrate our dynamic interaction, we consider an

arbitrary block (i.e., B_l , $l=1,2,\cdots$) in both branches. We first compute self-attention in block B_i of the SNN branch and the ANN branch to obtain attention weight maps, which can be summarized as follows:

$$W_l^e = \text{SoftMax}(\frac{Q_e K_e^{\top}}{\sqrt{d_e}} + \lambda_1 \mathcal{P} + \lambda_2 \mathcal{S}_e), \tag{1}$$

$$W_l^f = \operatorname{SoftMax}(\frac{Q_f K_f^{\top}}{\sqrt{d_f}} + \lambda_1 \mathcal{P} + \lambda_2 \mathcal{S}_f), \tag{2}$$

where $W_l^e, W_l^f \in \mathbb{R}^{nW \times M^2 \times M^2}$ are the attention weight maps for events and frames. Q_e, Q_f and K_e, K_f are queries and keys for the two modalities. \mathcal{P} refers to the relative positional embedding, and $\mathcal{S}_e, \mathcal{S}_f$ are relative semantic embeddings (see Sec.3.2). nW stands for the number of windows, and M is the window size. λ_1, λ_2 are two scalars to reweight \mathcal{P} and \mathcal{S} before adding to the attention weights.

In practice, the attention weight map from each modality is passed to the other and mapped to a unifying attention space using specially designed functions. This projection is necessary because, with multi-head attention, the weights resemble normal feature maps, treating the head dimension like a channel dimension and the attention weight maps for different modalities are distributed over different attention spaces. We refer to this meticulously handcrafted function as the attention kernel function, denoted as \mathcal{F} . A simple yet effective implementation of the attention kernel function can be mathematically described as:

$$\mathcal{F}(\boldsymbol{A}_{ij}) = \frac{1}{H} \sum_{h=1}^{H} \boldsymbol{A}_{ij}^{h}, \tag{3}$$

where H denotes the head number in multi-head self-attention, and $\mathbf{A} \in \mathbb{R}^{nW \times H \times M^2 \times M^2}$ is the attention weight map. Finally, we add the mapped attention weights to the attention weights of the other modality to obtain the final attention weights \mathcal{W}_I^e and \mathcal{W}_I^f as:

$$\mathcal{W}_l^e = W_l^e \oplus \lambda_3 \mathcal{F}_f(W_l^f), \tag{4}$$

$$\mathcal{W}_l^f = W_l^f \oplus \lambda_4 \mathcal{F}_e(W_l^e), \tag{5}$$

where \oplus denotes the element-wise sum operation. We use attention kernel functions \mathcal{F}_f and \mathcal{F}_e for frames and events respectively due to the disparity of their attention maps.

3.2. Semantic-Enhanced Swin Transformer

In HDI-Former, the ANN branch acts as the spatial feature encoder to extract fine static textures from frames. While the Swin Transformer [48] effectively exploits geometric information in images through relative positional embedding, relying solely on this aspect is insufficient [13, 38]. Thus, we introduce Relative Semantic Embedding, referred to as RSE, to improve data utilization and token correlations by explicitly integrating semantic information into

self-attention. Concretely, we first obtain the feature map $X \in \mathbb{R}^{N \times C}$ input to self-attention, where N is the sequence length and C is the channel dimension. Then, we compute the relative semantic distance between any two tokens by subtraction, which can be formulated as:

$$a_{ij} = X_i - X_j, i, j = 1, 2, \dots, N,$$
 (6)

where $a \in \mathbb{R}^{N \times N \times C}$ is the relative semantic distance matrix. Then we convert a to RSE using a Multi-Layer Perceptron (MLP) with a single output channel. Given there are only two semantic relations between tokens in object detection (i.e., belong to the same object or not), the RSE is supposed to be symmetric. Thus, we feed only the upper triangular part of a into the MLP and symmetrically populate the lower triangles with the resulting RSE. The abovementioned operations can be described as follows:

$$S_{ij} = W_m(W_m' a_{ij} + B_m') + B_m, i \le j, \tag{7}$$

where $S \in \mathbb{R}^{N \times N \times 1}$ denotes the proposed RSE. W_m, W_m' and B_m, B_m' are learnable weights.

Upon RSE, we introduce a novel self-attention mechanism called Semantic-Enhanced Multi-head Self-Attention (SEMSA). By replacing the original self-attention in the Swin Transformer with SEMSA, we create the Semantic-Enhanced Swin Transformer (SEST) as the ANN branch of our HDI-Former. SEST comprises multiple stacked blocks, each executing shifted window partitioning, SEMSA, and feed-forward (FFN) operations. Besides, layer normalization [70] and dropout [63] are also applied within each block. In summary, two consecutive blocks in our SEST can be formulated as follows:

$$\hat{Y}_l = \text{W-SEMSA}(\text{LN}(Y_{l-1})) + Y_{l-1}, \tag{8}$$

$$Y_l = \text{MLP}(\text{LN}(\hat{Y}_l)) + \hat{Y}_l, \tag{9}$$

$$\hat{Y}_{l+1} = \text{SW-SEMSA}(\text{LN}(Y_l)) + Y_l, \tag{10}$$

$$Y_{l+1} = \text{MLP}(\text{LN}(\hat{Y}_{l+1})) + \hat{Y}_{l+1},$$
 (11)

where $\hat{Y}_l, \hat{Y}_{l+1} \in \mathbb{R}^{N \times C}$ denote the outputs of W-SEMSA and SW-SEMSA modules. Y_l and Y_{l+1} are the outputs of the two blocks. W-SEMSA and SW-SEMSA represent window-based SEMSA with regular and shifted window partitioning configurations, respectively.

3.3. Spiking Swin Transformer

To efficiently process event streams with low energy consumption and enable dynamic interaction with the ANN branch, we design a novel spiking version of the Swin Transformer, which is the first trial to design a directly-trained SNN-based Transformer model for energy-efficient object detection. In contrast to ANN, SNN neurons transmit binary spikes for communication [76], so we need to

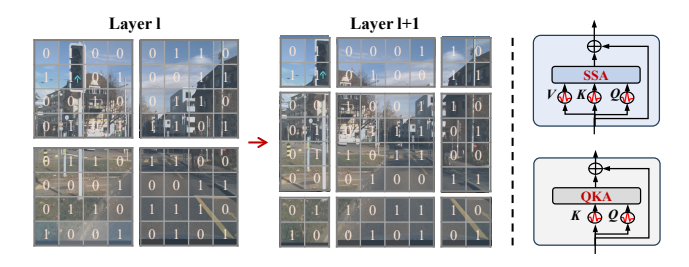


Figure 3. The spiked self-attention with shifted windows and two kinds of blocks in the Spiking Swin Transformer.

convert the feature map I into binary spikes and make the core self-attention mechanism compatible with spikes. To achieve this, we generate the binary feature map by adding a spiking neuron layer after the first convolutional layer in the patch splitting stage. Moreover, the Q, K, V produced by self-attention are quantized by binarization (see Fig. 3). Meanwhile, we introduce the Spiking Self-Attention (SSA) to extract the spiked feature maps. By removing softmax normalization, SSA completely avoids multiplications, aligning with the energy-efficient calculations of SNNs. The operational steps in our Spiking Swin Transformer can be mathematically represented as follows:

$$SSA'(X) = \mathcal{SN}((QK^{\top} \cdot s + \lambda_1 \mathcal{P} + \lambda_2 \mathcal{S}_e)V), \quad (12)$$

$$SSA(X) = \mathcal{SN}(BN(Linear(SSA'(X)))), \tag{13}$$

$$\hat{Z}_{l} = SSA(Z_{l-1}) + Z_{l-1}, \tag{14}$$

$$Z_l = \text{MLP}(\hat{Z}_l) + \hat{Z}_l, \tag{15}$$

where Q, K, V refer to spiked query, key, and value derived from X. \mathcal{SN} represents spiking neuron layer, and s is a scaling factor. \hat{Z}_l and Z_l are the output of SSA and the block. Batch normalization is implemented for reparameterization convolutions as [12] suggests.

Due to the need for a higher frequency of processing events compared to frames during asynchronous inference and the challenges in training SNNs, we propose a new training strategy for object detection regression tasks. In short, we introduce Q-K attention to make our Spiking Swin Transformer more efficient and easier to train. Q-K attention only uses two spike-form components query and key. By performing row summation, Q-K attention derives a token-wise attention vector $A_t \in \mathbb{R}^{N \times 1}$ from Q, which models the binary importance of different tokens. Then, Hadamard product \otimes is conducted between A_t and K. We can formulate these operations as follows:

$$A_t = \mathcal{SN}(\sum_{j=1}^D Q_{ij}), \tag{16}$$

$$QKA(\boldsymbol{X}) = A_t \otimes K, \tag{17}$$

where QKA stands for the Q-K attention operation. In real implementation, we utilize both QKA and SSA for a trade-off between speed and accuracy.

4. Experiments

4.1. Experimental Settings

Dataset. To verify the effectiveness of our HDI-Former, we conduct experiments primarily on the DSEC-Detection dataset [16]. It provides paired frames and events at a resolution of 640×480, along with 390k boxes at 20 Hz for object detection in driving scenarios. For fair comparisons, we also evaluate our Spiking Swin Transformer on the Gen1 dataset [59] which is widely used in SNNs for single-modality event-based object detection. The Gen1 dataset contains events at a resolution of 304×240 and 255k boxes with a frequency of 1 Hz, 2 Hz, or 4 Hz.

Implementation Details. We select the Swin Transformer-Tiny [48] (i.e., Swin-T) as the backbone owning to accuracy-speed trade-off. The patch size and window size are set to P = 4 and M = 8. In the ANN branch, we set the channel number of the hidden layers in the first stage C_a = 96, while the query dimension of each head is $d_a = 32$. For the convenience of training SNN, we reduce the number of channels to $C_s = 64$ and $d_s = 16$. The timestep in SNN is set to T = 5, and the number of blocks to perform dynamic interaction is $N_l = 4$. Following Swin Transformer, we use Mask R-CNN [22] as our detection head and utilize random resize as data augmentation. With batch size set to 16, we adopt an AdamW optimizer [31] with an initial learning rate of 10^{-4} and weight decay of 0.05. All experiments are conducted on NVIDIA A100 GPUs. We report the mean average precision (e.g., COCO mAP [42]) as evaluation metrics, containing mAP at IoU = 0.5 (i.e., mAP₅₀) and the average AP between 0.5 and 0.95 (i.e., mAP). We also compare the SNNs from the perspective of energy consumption.

4.2. Comparison with State-of-the-Art Methods

To verify the effectiveness of HDI-Former, we compare it with eleven state-of-the-art methods and four baselines in Table 1 and Fig. 4 to show the advantages of our hybrid framework from three perspectives.

Frame Modality. We present a comparison between our SEST branch and seven state-of-the-art methods, including Faster R-CNN [61], RetinaNet [43], CenterNet [75], YOLOv5 [79], YOLOv7 [68], ConvNeXt [49], and Swin Transformer [48]. Note that, our SEST outperforms the former six frame-based feedforward methods by a large margin. This is caused by the fact that the self-attention operation is better at extracting global features compared to standard convolution, indicating the potential of Transformer in the object detection task. Furthermore, by explicitly leveraging both geometric and semantic information, our SEST module comprehensively enhances the correlations between image tokens. Table 1 shows that our SEST achieves a remarkable mAP improvement of 0.8% with comparable parameters over the Swin Transformer.

Table 1. Comparison with state-of-the-art methods and our baselines* on the DSEC-Detection dataset [16]	[16].
---	-------

Modality	Method	Type	Backbone	Head	#Params	mAP ₅₀	mAP
	Faster R-CNN [61]	ANN	ResNet50+FPN	Faster R-CNN	41.9M	0.354	0.182
	RetinaNet [43]	ANN	ResNeXt-101-FPN	RetinaHead	53.9M	0.305	0.166
	CenterNet [75]	ANN	Hourglass-104	CenterNet	191.4M	0.351	0.204
RGB	YOLOv5 [79]	ANN	CSPDarknet53	YOLOv5	76.8M	0.332	0.209
KGB	YOLOv7 [68]	ANN	E-ELAN	YOLOv7	151.7M	0.315	0.182
	ConvNeXt [49]	ANN	ConvNeXt-T	Mask R-CNN	45.6M	0.462	0.248
	Swin Transformer [48]	ANN	Swin-T	Mask R-CNN	44.8M	0.487	0.269
	SEST*	ANN	Swin-T	Mask R-CNN	44.8M	0.504	0.277
	EMS-YOLO [65]	SNN	EMS-ResNet10	YOLOv3	6.2M	0.202	0.082
Event	Spiking Swin Transformer*	SNN	Swin QKFormer	YOLOv3	20.3M	0.254	0.116
	Swin Transformer*	ANN	Swin-T	YOLOv3	44.8M	0.266	0.133
	FPN-fusion [66]	ANN	ResNet-50	RetinaHead	/	0.289	0.152
	SFNet [50]	ANN	CSPDarknet53	YOLOv5	/	0.412	0.268
RGB +Events	HDI-Former*	Hybrid	Swin-T + Swin QKFormer	Mask R-CNN	64.2M	0.511	0.284
	SODFormer [35]	ANN	Deformable DETR	Deformable DETR	84.8M	0.513	0.284
	HDI-Former	Hybrid	Swin-T + Swin QKFormer	Mask R-CNN	64.2M	0.522	0.291

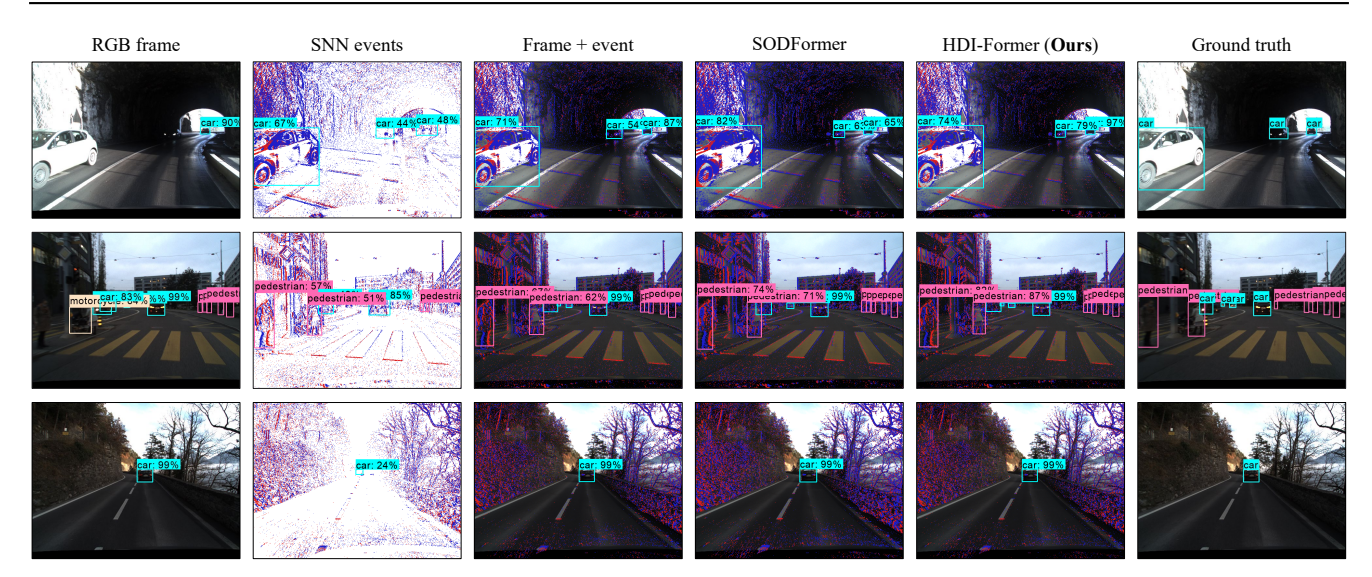


Figure 4. Representative examples of different object detection results in various scenarios on the DSEC-Detection dataset [16].

Event Modality. We compare our Spiking Swin Transformer in the SNN branch with EMS-YOLO [65] which achieves state-of-the-art performance among directly trained SNNs to the best of our knowledge. From the event modality in Table 1, our Spiking Swin Transformer achieves a significant mAP improvement of 3.4% over EMS-YOLO. In addition, our SNN branch performs relatively comparable to its ANN counterpart while significantly reducing energy consumption (see Sec.4.3).

Benefit From Multimodal Fusion. We further compare our HDI-Former with state-of-the-art multimodal methods (i.e., FPN-fusion [66], SFNet [50] and SODFormer [35]) and our baseline (i.e., HDI-Former* without dynamic interaction). Note that our HDI-Former outperforms FPN-fusion and SFNet by a large margin. Moreover, our HDI-Former, using the SNN branch to process the event stream, dramatically reduces energy consumption compared to SODFormer. Furthermore, we present some representative vi-

sualization results on the DSEC-Detection dataset [16] in Fig. 4. The three rows from top to bottom represent low-light, high-speed motion blur and static scenes, respectively. Obviously, our HDI-Former, making complementary use of frames and events, can perform robust object detection in various scenarios. The first row in Fig. 4 also shows that our HDI-Former, utilizing continuous event streams with rich temporal cues, successfully detects the occluded car on the left, overcoming single-frame object detection challenges.

4.3. Performance Evaluation of SNNs

Evaluation on Gen1 [10]. As illustrated in Table 2, we present a comparison of our Spiking Swin Transformer with some directly-trained SNN-based object detectors on the Gen1 dataset [10], the most widely used dataset for single-modality event-based object detection. We can find that our Spiking Swin Transformer achieves the best mAP of 0.291 and mAP $_{50}$ of 0.580 with the same timestep, which outper-

Table 2. Comparison of SNNs on the Gen1 dataset [10].

Model	Params	Firing Rate	Efficiency	mAP ₅₀	mAP
MS-ResNet18	9.49M	17.08%	2.43×	0.560	0.285
Sew-ResNet18	9.56M	18.80%	2.00×*	0.561	0.286
EMS-ResNet18	9.34M	20.09%	4.91×	0.565	0.286
Swin-T (ANN)	44.8M	/	/	0.588	0.296
Spiking Swin-T	20.3M	19.84%	6.34×	0.580	0.291

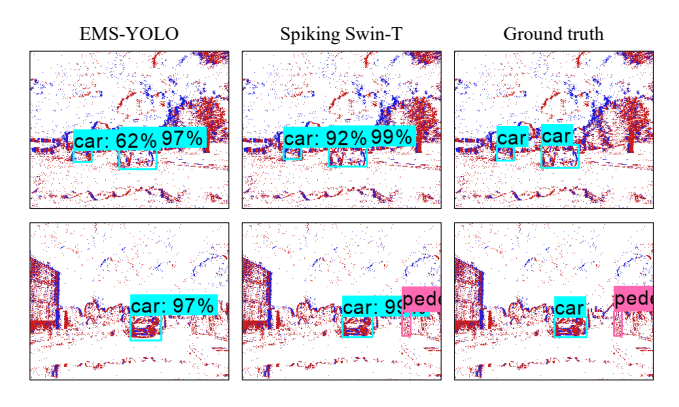


Figure 5. Representative visualization results of our SNN-branch and EMS-YOLO on the Gen1 dataset [10].

forms the state-of-the-art methods to our knowledge. It is worth noting that despite the higher performance achieved by the ANN counterpart, our Spiking Swin Transformer exploits a sparse representation with a spike firing rate of 19.84%, implying lower energy consumption. According to the quantitative formula for energy consumption in [65], we conclude that our Spiking Swin Transformer reduces up to 6.34× energy consumption compared to its ANN counterpart. Besides, some representative visualization results in Fig. 5 also indicate the effectiveness of our Spiking Swin Transformer on the Gen1 dataset [10].

Evaluation on DSEC-Detection [16]. As shown in Table 3, We further explore the effectiveness of our Spiking Swin Transformer on the DSEC-Detection dataset [16], which contains more classes of objects and is relatively more complex. By substituting CNN-based ResNet with the Swin Transformer which is more capable of modeling, our model gains greater expressive ability and outperforms EMS-YOLO [65] by a large margin of 3.4% mAP. Besides, our Spiking Swin Transformer maintains a low firing rate when facing more complicated data while EMS-YOLO increases significantly. As a result, the energy consumption can be saved up to $10.57 \times$ compared to ANN Swin Transformer. In other words, our SNN branch achieves comparable performance to the ANN with the same architecture while significantly reducing power consumption.

4.4. Ablation Study

Contribution of Each Component. We use the ANN Swin Transformer as the baseline to assess the contributions of each module. As illustrated in Table 4, three methods

Table 3. Comparison of SNNs on the DSEC-Detetection dataset.

Model	Firing Rate	Energy Consumption	mAP ₅₀	mAP
EMS-ResNet10	32.8%	8.18	0.202	0.082
Swin-T (ANN)	/	295.4	0.266	0.133
Spiking Swin-T	20.9%	27.95	0.254	0.116

Table 4. The contribution of each component to our HDI-Former on the DSEC-Detection dataset [16].

			Dynamic			Op	s(G)
Method	RSE	Events	Interaction	mAP ₅₀	mAP	AC	MAC
Baseline				0.487	0.269	0	98.6
(a)	\checkmark			0.504	0.277	0	99.5
(b)		\checkmark		0.511	0.284	26.12	100.17
HDI-Former		\checkmark	\checkmark	0.522	0.291	26.12	100.17

Table 5. The influence of SNN timesteps on the Gen1 dataset [10].

T	1	3	5	7	9
mAP ₅₀	0.565	0.572	0.580	0.568	0.564
mAP	0.286	0.289	0.291	0.288	0.286

namely (a), (b) and our HDI-Former consistently achieve higher performance by relying on the proposed components. To be specific, method (a), enhancing the correlations between tokens in self-attention by explicitly utilizing semantic information, obtains a 0.8% mAP improvement over the baseline. By involving events through the Spiking Swin Transformer, method (b) is capable of exploiting rich temporal cues from continuous event streams and making complementary use of frames and events, so the detection mAP is further enhanced by 0.7% compared to (a). By adopting dynamic interaction, our HDI-Former achieves an mAP improvement of 0.7% over method (b) and 1.4% over method (a). This reveals that our dynamic interaction mechanism favors complementary context capturing across frames and events while improving the model's capability to extract features at a more fundamental level during the feature extraction stage. Besides, our HDI-Former introduces few ACs and almost no MACs compared to the baseline, ensuring high accuracy and energy efficiency.

Influence of SNN Timesteps. To explore the impact of SNN timesteps, we report the performance of our Spiking Swin-T on the Gen1 dataset by first fixing the length of temporal window and then setting various timesteps T (see Table 5). Note that, the performance is subpar when T is 1 or 3 as the small timestep hinders feature extraction. Conversely, it may be unsatisfactory with a high timestep (e.g., T=7) due to increased training difficulty. The limited number of events within each timestep may also contribute to the inability to convey valid information when T is too large.

Influence of the Number of Interaction Layers. To further analyze the impact of dynamic interaction, we vary the number of layers where dynamic interaction is applied to 2, 4, 6, and 8, respectively, and evaluate the performance of

Table 6. The influence of the number of layers conducting dynamic interaction on the DSEC-Detection dataset [16].

Layers	0	2	4	6	8
mAP ₅₀	0.511	0.518	0.522	0.521	0.517
mAP	0.284	0.288	0.291	0.290	0.286

our HDI-Former. From Table 6, it's evident that our HDI-Former achieves optimal performance with 4 dynamic interaction layers (N_l = 4). This suggests that dynamic interaction increases the model's expressiveness. Interestingly, the performance seems to vary marginally across different numbers of dynamic interaction layers, implying that a few layers are sufficient to achieve our objectives.

4.5. Scalability Test

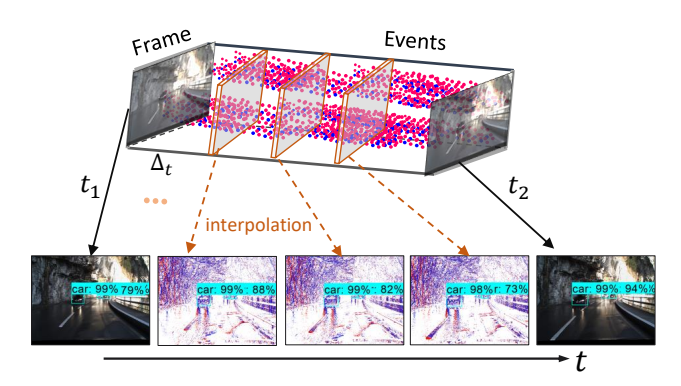


Figure 6. Visualization of asynchronous high-frequency inference through incorporating the continuous event stream.

Asynchronous Inference Validation. Conventional cameras with global shutters face limitations in output frame rate, resulting in gaps between adjacent frames. Our HDI-Former introduces an event stream of high temporal resolution to effectively fill these gaps and achieve continuous object detection. To achieve high-frequency detection, we first sample from the event stream using a sliding window of 0.05s length shifting forward by 0.0125s, resulting in an event stream of 80 Hz. We then input frames at 20 Hz and event temporal bins at 80 Hz into our HDI-Former to produce detections at 80 Hz. As depicted in Fig. 6, the middle three figures display the predictions, showing a smooth transition of the predicted box from the first frame to the second. This indicates that our HDI-Former can leverage the event stream of high temporal resolution to overcome the limitation of inference frequency and achieve continuous object detection in real-world applications.

Dynamic Interaction Analysis. To investigate the interpretability of the dynamic interaction mechanism, we present a scenario involving objects moving at different speeds in Fig. 7. We observe a car on the left experiencing high-speed motion blur, while a car in the middle appears static. The attention map reveals that the ANN branch fails to highlight the left object, and the event modality struggles

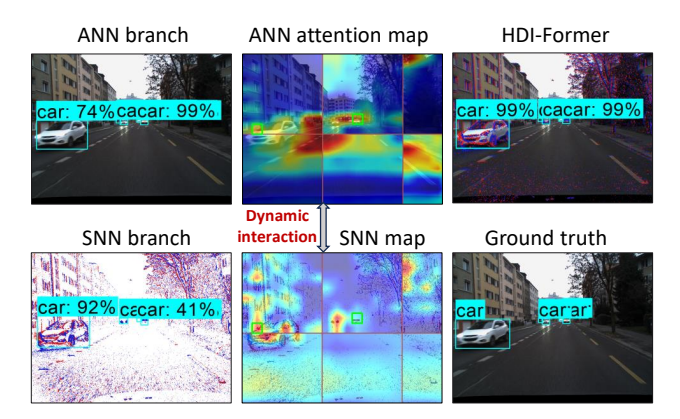


Figure 7. Representative instance verifying the necessity and effectiveness of dynamic interaction.

to recognize the middle object. However, these unattended regions contain valuable information crucial for accurate detection. Leveraging attention weights from each other, our dynamic interaction mechanism effectively addresses this challenge. In other words, the proposed dynamic interaction mechanism can leverage the complementarity of frames and events via cross-modality interaction.

5. Conclusion

This paper proposes a novel Hybrid Dynamic Interaction ANN-SNN Transformer, namely HDI-Former, which is a pioneering approach to integrate ANNs and SNNs to utilize their complementary strengths dynamically. To achieve this, we first present a novel semantic-enhanced self-attention mechanism to strengthen the correlation between tokens in the ANN branch. Then an energy-efficient Spiking Swin Transformer branch is proposed to extract temporal cues from events. Finally, the dynamic interaction mechanism enables cross-modality interaction between the ANN and SNN. Experimental results demonstrate that our HDI-Former significantly surpasses the state-of-the-art methods and the SNN branch achieves comparable performance to the ANN counterpart at lower energy consumption. To our knowledge, this is the first attempt to directly train a hybrid ANN-SNN Transformer for high-accuracy energy-efficient multimodal object detection. We believe that conducting effective cross-modality interaction is an exciting breakthrough in object detection with frames and events, inspiring directions for future research.

Limitation. The power consumption is simulated based on existing academic papers rather than neuromorphic chips, potentially increasing inference time and skewing power usage estimates. Future research will focus on deploying algorithms onto neuromorphic chips to meet the high-speed and energy-efficient requirements of event cameras.

References

- [1] Soikat Hasan Ahmed, Jan Finkbeiner, and Emre Neftci. A hybrid snn-ann network for event-based object detection with spatial and temporal attention. *arXiv preprint arXiv:2403.10173*, 2024. 3
- [2] Asude Aydin, Mathias Gehrig, Daniel Gehrig, and Davide Scaramuzza. A hybrid ann-snn architecture for low-power and low-latency visual perception. In arXiv, 2023. 2, 3
- [3] Lennard Bodden, Franziska Schwaiger, Duc Bach Ha, Lars Kreuzberg, and Sven Behnke. Spiking centernet: A distillation-boosted spiking neural network for object detection. In arXiv, 2024. 2
- [4] Christian Brandli, Raphael Berner, Minhao Yang, Shih-Chii Liu, and Tobi Delbruck. A 240× 180 130 db 3 μs latency global shutter spatiotemporal vision sensor. *IEEE Journal of Solid-State Circuits*, 49(10):2333–2341, 2014. 1, 3
- [5] Hu Cao, Guang Chen, Jiahao Xia, Genghang Zhuang, and Alois Knoll. Fusion-based feature attention gate component for vehicle detection based on event camera. *IEEE Sensors Journal*, 21(21):24540–24548, 2021. 1, 2
- [6] Jiahang Cao, Xu Zheng, Yuanhuiyi Lyu, Jiaxu Wang, Renjing Xu, and Lin Wang. Chasing day and night: Towards robust and efficient all-day object detection guided by an event camera. In arXiv, 2023. 1
- [7] Biswadeep Chakraborty, Xueyuan She, and Saibal Mukhopadhyay. A fully spiking hybrid neural network for energy-efficient object detection. *IEEE Transactions on Image Processing*, 30:9014–9029, 2021. 2
- [8] Nicholas FY Chen. Pseudo-labels for supervised learning on dynamic vision sensor data, applied to object detection under ego-motion. In *Proceedings of the IEEE conference on Computer Vision and Pattern Recognition Workshops*, pages 644–653, 2018. 1
- [9] Loïc Cordone, Benoît Miramond, and Philippe Thierion. Object detection with spiking neural networks on automotive event data. In *Proceedings of the International Joint Conference on Neural Networks*, pages 1–8, 2022. 2
- [10] Pierre De Tournemire, Davide Nitti, Etienne Perot, Davide Migliore, and Amos Sironi. A large scale event-based detection dataset for automotive. In arXiv, 2020. 6, 7
- [11] Lei Deng, Yujie Wu, Xing Hu, Ling Liang, Yufei Ding, Guoqi Li, Guangshe Zhao, Peng Li, and Yuan Xie. Rethinking the performance comparison between snns and anns. *Neural networks*, 121:294–307, 2020. 2
- [12] Xiaohan Ding, Xiangyu Zhang, Ningning Ma, Jungong Han, Guiguang Ding, and Jian Sun. Repvgg: Making vgg-style convnets great again. In Proceedings of the IEEE/CVF conference on computer vision and pattern recognition, pages 13733–13742, 2021. 5
- [13] Alexey Dosovitskiy, Lucas Beyer, Alexander Kolesnikov, Dirk Weissenborn, Xiaohua Zhai, Thomas Unterthiner, Mostafa Dehghani, Matthias Minderer, Georg Heigold, Sylvain Gelly, et al. An image is worth 16x16 words: Transformers for image recognition at scale. In *Proceedings of the International Conference on Learning Representations*, 2020, 4

- [14] Yimeng Fan, Wei Zhang, Changsong Liu, Mingyang Li, and Wenrui Lu. Sfod: Spiking fusion object detector. In Proceedings of the IEEE/CVF International Conference on Computer Vision, 2024. 2
- [15] Guillermo Gallego, Tobi Delbrück, Garrick Orchard, Chiara Bartolozzi, Brian Taba, Andrea Censi, Stefan Leutenegger, Andrew J Davison, Jörg Conradt, Kostas Daniilidis, et al. Event-based vision: A survey. *IEEE Transactions on Pattern* Analysis and Machine Intelligence, 44(1):154–180, 2020. 1
- [16] Daniel Gehrig and Davide Scaramuzza. Low latency automotive vision with event cameras. *Nature*, 2024. 5, 6, 7, 8, 1, 3, 4
- [17] Daniel Gehrig, Antonio Loquercio, Konstantinos G Derpanis, and Davide Scaramuzza. End-to-end learning of representations for asynchronous event-based data. In *Proceedings of the IEEE/CVF International Conference on Computer Vision*, pages 5633–5643, 2019. 1
- [18] Daniel Gehrig, Michelle Rüegg, Mathias Gehrig, Javier Hidalgo-Carrió, and Davide Scaramuzza. Combining events and frames using recurrent asynchronous multimodal networks for monocular depth prediction. *IEEE Robotics and Automation Letters*, 6(2):2822–2829, 2021. 1
- [19] Mathias Gehrig and Davide Scaramuzza. Recurrent vision transformers for object detection with event cameras. In Proceedings of the IEEE/CVF Conference on Computer Vision and Pattern Recognition, pages 13884–13893, 2023. 3, 1
- [20] Menghan Guo, Shoushun Chen, Zhe Gao, Wenlei Yang, Peter Bartkovjak, Qing Qin, Xiaoqin Hu, Dahai Zhou, Qiping Huang, Masayuki Uchiyama, et al. A three-wafer-stacked hybrid 15-mpixel cis +1-mpixel evs with 4.6-gevent/s readout, in-pixel tdc, and on-chip isp and esp function. *IEEE Journal of Solid-State Circuits*, 2023. 1, 3
- [21] Bing Han and Kaushik Roy. Deep spiking neural network: Energy efficiency through time based coding. In *Proceedings* of the European Conference on Computer Vision, pages 388– 404, 2020. 2
- [22] Kaiming He, Georgia Gkioxari, Piotr Dollár, and Ross Girshick. Mask r-cnn. In *Proceedings of the IEEE International Conference on Computer Vision*, pages 2961–2969, 2017. 5
- [23] Yuhuang Hu, Tobi Delbruck, and Shih-Chii Liu. Learning to exploit multiple vision modalities by using grafted networks. In *Proceedings of the European Conference on Computer Vision*, pages 85–101, 2020. 2
- [24] Yangfan Hu, Qian Zheng, Xudong Jiang, and Gang Pan. Fast-snn: Fast spiking neural network by converting quantized ann. IEEE Transactions on Pattern Analysis and Machine Intelligence, 2023.
- [25] Massimiliano Iacono, Stefan Weber, Arren Glover, and Chiara Bartolozzi. Towards event-driven object detection with off-the-shelf deep learning. In *Proceedings of the IEEE/RSJ International Conference on Intelligent Robots and Systems (IROS)*, pages 1–9, 2018. 2
- [26] Yu Jiang, Yuehang Wang, Minghao Zhao, Yongji Zhang, and Hong Qi. Nighttime traffic object detection via adaptively integrating event and frame domains. *Fundamental Research*, 2023. 1, 2

- [27] Zhuangyi Jiang, Pengfei Xia, Kai Huang, Walter Stechele, Guang Chen, Zhenshan Bing, and Alois Knoll. Mixed frame-/event-driven fast pedestrian detection. In *Proceedings of the International Conference on Robotics and Automation*, pages 8332–8338, 2019. 1, 2
- [28] Zhaodong Kang, Jianing Li, Lin Zhu, and Yonghong Tian. Retinomorphic sensing: A novel paradigm for future multimedia computing. In *Proceedings of the 29th ACM Inter*national Conference on Multimedia, pages 144–152, 2021.
- [29] Salman Khan, Muzammal Naseer, Munawar Hayat, Syed Waqas Zamir, Fahad Shahbaz Khan, and Mubarak Shah. Transformers in vision: A survey. ACM Computing Surveys, 54(10s):1–41, 2022. 2
- [30] Seijoon Kim, Seongsik Park, Byunggook Na, and Sungroh Yoon. Spiking-yolo: Spiking neural network for energyefficient object detection. In *Proceedings of the AAAI con*ference on artificial intelligence, pages 11270–11277, 2020.
- [31] Diederik P Kingma and Jimmy Ba. Adam: A method for stochastic optimization. In *Proceedings of the International Conference on Learning Representations*, pages 1–15, 2014.
- [32] Kazutoshi Kodama, Yusuke Sato, Yuhi Yorikado, Raphael Berner, Kyoji Mizoguchi, Takahiro Miyazaki, Masahiro Tsukamoto, Yoshihisa Matoba, Hirotaka Shinozaki, Atsumi Niwa, et al. 1.22 μm 35.6 mpixel rgb hybrid event-based vision sensor with 4.88 μm-pitch event pixels and up to 10k event frame rate by adaptive control on event sparsity. In *Proceedings of the IEEE International Solid-State Circuits Conference*, pages 92–94, 2023. 1, 3
- [33] Alexander Kugele, Thomas Pfeil, Michael Pfeiffer, and Elisabetta Chicca. Hybrid snn-ann: Energy-efficient classification and object detection for event-based vision. In *Proceedings of the DAGM German Conference on Pattern Recognition*, pages 297–312, 2021. 3
- [34] Chankyu Lee, Adarsh Kumar Kosta, Alex Zihao Zhu, Kenneth Chaney, Kostas Daniilidis, and Kaushik Roy. Spike-flownet: Event-based optical flow estimation with energy-efficient hybrid neural networks. In *Proceedings of the European Conference on Computer Vision*, pages 366–382, 2020.
- [35] Dianze Li, Jianing Li, and Yonghong Tian. Sodformer: Streaming object detection with transformer using events and frames. *IEEE Transactions on Pattern Analysis and Machine Intelligence*, 2023. 1, 2, 3, 6, 4
- [36] Jianing Li, Siwei Dong, Zhaofei Yu, Yonghong Tian, and Tiejun Huang. Event-based vision enhanced: A joint detection framework in autonomous driving. In *Proceedings of* the IEEE International Conference on Multimedia and Expo, pages 1396–1401, 2019. 1, 2
- [37] Jianing Li, Jia Li, Lin Zhu, Xijie Xiang, Tiejun Huang, and Yonghong Tian. Asynchronous spatio-temporal memory network for continuous event-based object detection. *IEEE Transactions on Image Processing*, 31:2975–2987, 2022. 2,
- [38] Jingyu Li, Zhendong Mao, Shancheng Fang, and Hao Li. Er-san: Enhanced-adaptive relation self-attention network

- for image captioning. In *Proceedings of the International Joint Conference on Artificial Intelligence*, pages 1081–1087, 2022. 4
- [39] Lei Li, Alexander Liniger, Mario Millhaeusler, Vagia Tsiminaki, Yuanyou Li, and Dengxin Dai. Object-centric crossmodal feature distillation for event-based object detection. In arXiv, 2023. 1
- [40] Yang Li, Xiang He, Yiting Dong, Qingqun Kong, and Yi Zeng. Spike calibration: Fast and accurate conversion of spiking neural network for object detection and segmentation. In arXiv, 2022. 2
- [41] Yuhang Li, Tamar Geller, Youngeun Kim, and Priyadarshini Panda. Seenn: Towards temporal spiking early exit neural networks. *Proceedings of the Advances in Neural Information Processing Systems*, 36, 2024. 2
- [42] Tsung-Yi Lin, Michael Maire, Serge Belongie, James Hays, Pietro Perona, Deva Ramanan, Piotr Dollár, and C Lawrence Zitnick. Microsoft coco: Common objects in context. In Proceedings of the European Conference on Computer Vision, pages 740–755, 2014. 5
- [43] Tsung-Yi Lin, Priya Goyal, Ross Girshick, Kaiming He, and Piotr Dollár. Focal loss for dense object detection. In Proceedings of the IEEE International Conference on Computer Vision, pages 2980–2988, 2017. 5, 6
- [44] Faqiang Liu and Rong Zhao. Enhancing spiking neural networks with hybrid top-down attention. Frontiers in Neuroscience, 16:949142, 2022. 3
- [45] Mason Liu and Menglong Zhu. Mobile video object detection with temporally-aware feature maps. In *Proceedings of the IEEE conference on computer vision and pattern recognition*, pages 5686–5695, 2018. 3
- [46] Mengyun Liu, Na Qi, Yunhui Shi, and Baocai Yin. An attention fusion network for event-based vehicle object detection. In *Proceedings of the IEEE International Conference on Image Processing*, pages 3363–3367, 2021. 1, 2
- [47] Wei Liu, Dragomir Anguelov, Dumitru Erhan, Christian Szegedy, Scott Reed, Cheng-Yang Fu, and Alexander C Berg. Ssd: Single shot multibox detector. In *Proceedings* of the European Conference on Computer Vision, pages 21– 37, 2016. 1
- [48] Ze Liu, Yutong Lin, Yue Cao, Han Hu, Yixuan Wei, Zheng Zhang, Stephen Lin, and Baining Guo. Swin transformer: Hierarchical vision transformer using shifted windows. In *Proceedings of the IEEE/CVF international conference on computer vision*, pages 10012–10022, 2021. 3, 4, 5, 6
- [49] Zhuang Liu, Hanzi Mao, Chao-Yuan Wu, Christoph Feichtenhofer, Trevor Darrell, and Saining Xie. A convnet for the 2020s. In *Proceedings of the IEEE/CVF conference on com*puter vision and pattern recognition, pages 11976–11986, 2022. 5, 6
- [50] Zhanwen Liu, Nan Yang, Yang Wang, Yuke Li, Xiangmo Zhao, and Fei-Yue Wang. Enhancing traffic object detection in variable illumination with rgb-event fusion. In arXiv, 2023. 1, 6
- [51] Cai Luo, Jihua Wu, Shixin Sun, and Peng Ren. Transcodnet: Underwater transparently camouflaged object detection via rgb and event frames collaboration. *IEEE Robotics and Automation Letters*, 2023. 1, 2

- [52] Wolfgang Maass. Networks of spiking neurons: the third generation of neural network models. *Neural networks*, 10 (9):1659–1671, 1997. 2
- [53] Diederik Paul Moeys, Federico Corradi, Chenghan Li, Simeon A Bamford, Luca Longinotti, Fabian F Voigt, Stewart Berry, Gemma Taverni, Fritjof Helmchen, and Tobi Delbruck. A sensitive dynamic and active pixel vision sensor for color or neural imaging applications. *IEEE Transactions on Biomedical Circuits and Systems*, 12(1):123–136, 2017. 1, 3
- [54] Emre O Neftci, Hesham Mostafa, and Friedemann Zenke. Surrogate gradient learning in spiking neural networks: Bringing the power of gradient-based optimization to spiking neural networks. *IEEE Signal Processing Magazine*, 36 (6):51–63, 2019. 2, 1
- [55] Antje Nuthmann and Teresa Canas-Bajo. Visual search in naturalistic scenes from foveal to peripheral vision: A comparison between dynamic and static displays. *Journal of Vi*sion, 22(1):1–10, 2022. 3
- [56] Yansong Peng, Yueyi Zhang, Peilin Xiao, Xiaoyan Sun, and Feng Wu. Better and faster: Adaptive event conversion for event-based object detection. In *Proceedings of the AAAI Conference on Artificial Intelligence*, pages 2056–2064, 2023. 2
- [57] Yansong Peng, Yueyi Zhang, Zhiwei Xiong, Xiaoyan Sun, and Feng Wu. Get: group event transformer for event-based vision. In *Proceedings of the IEEE/CVF International Conference on Computer Vision*, pages 6038–6048, 2023. 3
- [58] Yansong Peng, Hebei Li, Yueyi Zhang, Xiaoyan Sun, and Feng Wu. Scene adaptive sparse transformer for event-based object detection. In Proceedings of the IEEE/CVF Conference on Computer Vision and Pattern Recognition, pages 16794–16804, 2024. 1
- [59] Etienne Perot, Pierre De Tournemire, Davide Nitti, Jonathan Masci, and Amos Sironi. Learning to detect objects with a 1 megapixel event camera. *Proceedings of the Advances* in Neural Information Processing Systems, 33:16639–16652, 2020. 2, 5
- [60] Joseph Redmon and Ali Farhadi. Yolov3: An incremental improvement. In arXiv, 2018. 1
- [61] Shaoqing Ren, Kaiming He, Ross Girshick, and Jian Sun. Faster r-cnn: Towards real-time object detection with region proposal networks. In *Proceedings of the Advances in Neural Information Processing Systems*, 2015. 5, 6, 3
- [62] Kaushik Roy, Akhilesh Jaiswal, and Priyadarshini Panda. Towards spike-based machine intelligence with neuromorphic computing. *Nature*, 575(7784):607–617, 2019.
- [63] Nitish Srivastava, Geoffrey Hinton, Alex Krizhevsky, Ilya Sutskever, and Ruslan Salakhutdinov. Dropout: a simple way to prevent neural networks from overfitting. *The Journal of Machine Learning Research*, 15(1):1929–1958, 2014. 4
- [64] Emma EM Stewart, Matteo Valsecchi, and Alexander C Schütz. A review of interactions between peripheral and foveal vision. *Journal of Vision*, 20(12):2–2, 2020. 2, 3
- [65] Qiaoyi Su, Yuhong Chou, Yifan Hu, Jianing Li, Shijie Mei, Ziyang Zhang, and Guoqi Li. Deep directly-trained spiking neural networks for object detection. In *Proceedings* of the IEEE/CVF International Conference on Computer Vision, pages 6555–6565, 2023. 2, 6, 7, 1

- [66] Abhishek Tomy, Anshul Paigwar, Khushdeep S Mann, Alessandro Renzaglia, and Christian Laugier. Fusing eventbased and rgb camera for robust object detection in adverse conditions. In *Proceedings of the International Conference* on Robotics and Automation, pages 933–939, 2022. 1, 6
- [67] Sai Vemprala, Sami Mian, and Ashish Kapoor. Representation learning for event-based visuomotor policies. *Proceed*ings of the Advances in Neural Information Processing Systems, 34:4712–4724, 2021. 1
- [68] Chien-Yao Wang, Alexey Bochkovskiy, and Hong-Yuan Mark Liao. Yolov7: Trainable bag-of-freebies sets new state-of-the-art for real-time object detectors. In *Proceedings of the IEEE/CVF conference on computer vision and pattern recognition*, pages 7464–7475, 2023. 5, 6
- [69] Dongsheng Wang, Xu Jia, Yang Zhang, Xinyu Zhang, Yaoyuan Wang, Ziyang Zhang, Dong Wang, and Huchuan Lu. Dual memory aggregation network for event-based object detection with learnable representation. In *Proceed*ings of the AAAI Conference on Artificial Intelligence, pages 2492–2500, 2023. 2
- [70] Jingjing Xu, Xu Sun, Zhiyuan Zhang, Guangxiang Zhao, and Junyang Lin. Understanding and improving layer normalization. In Proceedings of the Advances in Neural Information Processing Systems, 2019. 4
- [71] Zheyu Yang, Yujie Wu, Guanrui Wang, Yukuan Yang, Guoqi Li, Lei Deng, Jun Zhu, and Luping Shi. Dashnet: A hybrid artificial and spiking neural network for high-speed object tracking. In arXiv, 2019. 2, 3
- [72] Mengwen Yuan, Chengjun Zhang, Ziming Wang, Huixiang Liu, Gang Pan, and Huajin Tang. Trainable spiking-yolo for low-latency and high-performance object detection. *Neural Networks*, 172:106092, 2024. 2
- [73] Rong Zhao, Zheyu Yang, Hao Zheng, Yujie Wu, Faqiang Liu, Zhenzhi Wu, Lukai Li, Feng Chen, Seng Song, Jun Zhu, et al. A framework for the general design and computation of hybrid neural networks. *Nature Communications*, 13(1): 3427, 2022. 2, 3
- [74] Chenlin Zhou, Han Zhang, Zhaokun Zhou, Liutao Yu, Liwei Huang, Xiaopeng Fan, Li Yuan, Zhengyu Ma, Huihui Zhou, and Yonghong Tian. Qkformer: Hierarchical spiking transformer using qk attention. In arXiv, 2024. 2
- [75] Xingyi Zhou, Dequan Wang, and Philipp Krähenbühl. Objects as points. In *arXiv*, 2019. 5, 6
- [76] Zhaokun Zhou, Yuesheng Zhu, Chao He, Yaowei Wang, YAN Shuicheng, Yonghong Tian, and Li Yuan. Spikformer: When spiking neural network meets transformer. In *Proceedings of the Eleventh International Conference on Learning Representations*, 2022. 4
- [77] Zhuyun Zhou, Zongwei Wu, Rémi Boutteau, Fan Yang, Cédric Demonceaux, and Dominique Ginhac. Rgb-event fusion for moving object detection in autonomous driving. In *Proceedings of the IEEE International Conference on Robotics and Automation*, pages 7808–7815, 2023. 1
- [78] Lin Zhu, Xiao Wang, Yi Chang, Jianing Li, Tiejun Huang, and Yonghong Tian. Event-based video reconstruction via potential-assisted spiking neural network. In *Proceedings of the IEEE/CVF Conference on Computer Vision and Pattern Recognition*, pages 3594–3604, 2022. 2

- [79] Xingkui Zhu, Shuchang Lyu, Xu Wang, and Qi Zhao. Tphyolov5: Improved yolov5 based on transformer prediction head for object detection on drone-captured scenarios. In Proceedings of the IEEE/CVF International Conference on Computer Vision, pages 2778–2788, 2021. 5, 6
- [80] Nikola Zubić, Daniel Gehrig, Mathias Gehrig, and Davide Scaramuzza. From chaos comes order: Ordering event representations for object detection. In *Proceedings of the IEEE/CVF Conference on Computer Vision and Pattern Recognition*, 2023. 2
- [81] Nikola Zubic, Mathias Gehrig, and Davide Scaramuzza. State space models for event cameras. In *Proceedings of the IEEE/CVF Conference on Computer Vision and Pattern Recognition*, pages 5819–5828, 2024. 1

HDI-Former: Hybrid Dynamic Interaction ANN-SNN Transformer for Object Detection Using Frames and Events

Supplementary Material

Table 7. Comparison with state-of-the-art methods on the DSEC-Detection dataset [16] involving only 2 classes.

Modality	Method	Type Backbone		mAP ₅₀	mAP
	RVT [19]	ANN	Transformer+RNN	0.587	0.384
Event	SAST [58]	ANN	Transformer	0.601	0.381
	SSM [81]	ANN	Transformer+SSM	0.552	0.380
	DAGr-18 [16]	ANN	GNN+CNN	-	0.376
Frame+Event	DAGr-34 [16]	ANN	GNN+CNN	-	0.390
Frame+Event	DAGr-50 [16]	ANN	GNN+CNN	0.660	0.419
	HDI-Former	ANN+SNN	Transformer	0.691	0.467

A. Detailed DSEC-Detection Dataset

The DSEC-Detection [16] dataset is collected using 2× Prophesee Gen3.1 cameras with a spatial resolution of 640×480 pixels. It includes detection labels for 60 hybrid sequences amounting to 70,379 frames and 390,118 bounding boxes. It is then divided into 47 sequences for training and 13 for testing. The labels are produced by applying an advanced object tracking algorithm and manually reviewing and adjusting to eliminate any incorrect tracks. There exist 8 classes, i.e., pedestrian, rider, car, bus, truck, bicycle, motorcycle, and train. *Notably, the results in the* main text are all evaluated on the full 8 classes, while some of the methods [16] involve only 2 classes (i.e., including only pedestrians and grouping cars, trucks, and buses as cars). For comprehensiveness, we further compare HDI-Former with several state-of-the-art methods on the DSEC-Detection dataset with the two-class setup in Table 7. The results show that HDI-Former achieves significant performance improvement against the other methods with mAP increases by 4.8% compared to the second optimal method. Furthermore, HDI-Former utilizes the energyefficient Spiking Swin Transformer to extract temporal cues from event streams, which reduces energy consumption.

B. Preliminaries

B.1. Event Camera Sensing Mechanism

Event cameras, called neuromorphic cameras, report pixelwise values of +1 or -1 for positive or negative log intensity differences, respectively. Each event e_n can be described as a four-attribute tuple (x_n,y_n,t_n,p_n) , which is generated for a pixel $u=(x_n,y_n)$ at the timestamp t_n once the log-intensity change exceeds the processing threshold θ_{th} , and it can be depicted as:

$$\ln R(\boldsymbol{u}_n, t_n) - \ln R(\boldsymbol{u}_n, t_n - \Delta t_n) = p_n \theta_{th}, \quad (18)$$

where Δt_n is the temporal sampling interval at a pixel, and the polarity $p_n \in \{-1, 1\}$ represents the increasing or decreasing change in the brightness, respectively.

Consequently, asynchronous events $S = \{e_n\}_{n=1}^{N_e}$ are sparse and discrete points in the spatio-temporal window Γ , which can be mathematically described as:

$$S(x, y, t) = \{p_n \delta(x - x_n, y - y_n, t - t_n)\}_{n=1}^{N_e}, \quad (19)$$

where N_e is the number of events during the spatiotemporal window Γ , and $\delta(\cdot)$ refers to the Dirac delta function, with $\delta(t)=0, \forall t\neq 0$, and $\int \delta(t)dt=1$. Event cameras offer the advantages of low latency, high dynamic range, and low redundancy.

B.2. Theory of Spiking Neural Networks

In SNNs, spiking neurons are the basic units with more biological plausibility as they mimic the membrane potential dynamics and the spiking communication scheme [65]. We choose the Leaky Integrate-and-Fire (LIF) model as the spiking neuron in our work as a good trade-off between bioplausibility and complexity. The dynamics of a LIF neuron can be formulated as:

$$H(t) = V(t-1) + \frac{1}{\tau}(X(t) - (V(t-1) - V_{reset})), (20)$$

$$S(t) = \Theta(H(t) - V_{th}), \tag{21}$$

$$V(t) = H(t)(1 - S(t)) + V_{reset}S(t),$$
 (22)

where τ is the membrane time constant, and X(t) is the current input at time step t. Whenever the membrane potential H(t) exceeds the firing threshold V_{th} , the spiking neuron triggers a spike S(t). $\Theta(v)$ is the Heaviside step function, which equals 1 when $v \leq 0$ and 0 otherwise. V(t) represents the membrane potential after the triggered event, which equals H(t) if no spike is generated and otherwise equals the reset potential V_{reset} . We can observe that LIF neurons are charged by input stimuli and remain at resting potential at other moments, which accounts for their high efficiency and low energy consumption.

Eq. 21 can be interpreted as a recurrent neural network that can be unrolled over multiple forward Euler steps and then trained using backpropagation through time. However, the Heaviside step function $\Theta(v)$ is not differentiable near 0 which impedes backpropagation. To solve this problem, we use surrogate gradients [54] to replace the gradient of the Heaviside function with the approximate function as:

$$\Theta(v) \approx \frac{1}{1 + (\pi v)^2}. (23)$$

	Downsp. rate (output size)	Layer name	ANN branch	SNN branch
Stage 1	4×	Patch Embedding	concat 4×4, 96-d, LN	concat 4×4 , 64 -d, BN, \mathcal{SN}
Stage 1	(120×160)	SEST / Swin QKFormer	$\begin{bmatrix} win. sz. 8 \times 8, \\ dim 96, head 3 \end{bmatrix} \times 2$	$\begin{bmatrix} win. sz. 8 \times 8, \\ dim 64, head 4 \end{bmatrix} \times 2$
Stage 2	8×	Patch Merging	concat 2×2, 192-d, LN	concat 2×2 , 128 -d, BN, \mathcal{SN}
Stage 2	(60×80)	SEST / Swin QKFormer	$ \begin{array}{c c} win. sz. 8 \times 8, \\ dim 192, head 6 \end{array} \times 2 $	win. sz. 8×8 , dim 128, head 8×2
Stage 2	16×	Patch Merging	concat 2×2, 384-d, LN	concat 2×2 , 256 -d, BN, \mathcal{SN}
Stage 3	(30×40)	SEST / Swin Spikformer	$\begin{bmatrix} win. sz. 8 \times 8, \\ dim 384, head 12 \end{bmatrix} \times 6$	$\begin{bmatrix} win. sz. 8 \times 8, \\ dim 256, head 16 \end{bmatrix} \times 6$
Stage 4	32×	Patch Merging	concat 2×2, 768-d, LN	concat 2×2 , 512 -d, BN, \mathcal{SN}
Stage 4	(15×20)	SEST / Swin Spikformer	win. sz. 8×8, dim 768, head 24 × 2	$\begin{array}{ c c c c c c c c c c c c c c c c c c c$

Table 8. Detailed architecture specifications of the HDI-Former.

SNNs showcase energy-efficient properties with neurons engaging in Accumulation Calculation (AC) operations exclusively during spikes. Hence, the energy consumption of SNNs is a vital metric which can be calculated [65] as:

$$E_{SNN} = \sum_{n=1}^{N_b} T_n \left(f_n \cdot E_A \cdot OP_A^n + E_M \cdot OP_M^n \right), \quad (24)$$

where T_n and f_n are the total time steps and the firing rate in the n-th block, respectively. OP_A^n and OP_M^n represent the number of accumulation calculation operations (AC) and Multiply-Accumulate (MAC) operations in the n-th block. E_A and E_M denote the computational energy of each operation and directly reference the power consumption of a neuromorphic chip with specific nanometer (nm) technology. In this work, we assume that various operations involved are 32-bit floating-point implemented in 45nm technology, where $E_A = 0.9 \mathrm{pJ}$ and $E_M = 4.6 \mathrm{pJ}$.

C. Detailed Network Architecture

C.1. Network Specifications

We show more details of the network architecture in Table 8. It can be seen that we set the architectures of the two branches approximately the same to ensure dynamic interaction. The output sizes are obtained presuming a 640×480 input which is exactly the case in the DSEC-Detection dataset. "concat $n \times n$ " represents splitting the feature map into patches of size n and merging the features within each patch into a token, which results in downsampling of feature map by a rate of n. In the ANN branch, we achieve this through a Conv2D layer with kernel size and stride both set to P in the patch embedding stage, while patch merging is

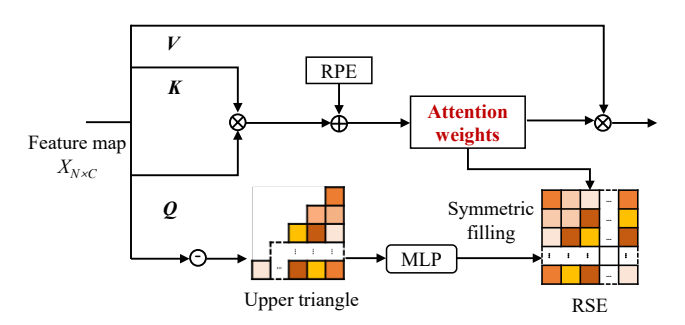


Figure 8. The framework of computing the Relative Semantic Embedding (i.e. RSE). We first obtain the relative semantic distance matrix by subtraction and convert it to the RSE with MLP. We use only the upper triangle of the distance matrix to ensure symmetry.

achieved by concatenating the neighboring $n \times n$ tokens and reducing the channels by 2 with a Linear layer. In the SNN branch, we follow [74] to use a {Conv2D-BN-MaxPooling- \mathcal{SN} } combination for downsampling with a shortcut connection for both patch embedding and patch merging stage. Note that we add an extra {Conv2D-BN- \mathcal{SN} } layer before the patch embedding stage of the SNN branch to transform the input into spikes.

C.2. Framework of Relative Semantic Embedding

For a more intuitive clarification of the proposed Relative Semantic Embedding (i.e., RSE), we show its computational procedure in Fig. 8. The upper part of Fig. 8 indicates the computation of the original self-attention in Swin Transformer. On the bottom part, we calculate the relative semantic distance between any two tokens $a \in \mathbb{R}^{N \times N \times C}$ by subtraction as formulated in Eq. 6. We denote this subtraction operation by the notation \ominus in Fig. 8. After that, we convert a to RSE through an MLP with the output channel

Table 9. Com	parison with	state-of-the-art	methods and	baselines* o	on the l	PKU-DAVIS-	-SOD dataset [351.

Modality	Method	Backbone	Temporal	mAP_{50}	Runtime (ms)
	Faster R-CNN [61]	ResNet50+FPN	No	0.443	11.6
RGB	LSTM-SSD [45]	Bottleneck-LSTM	Yes	0.456	22.4
KUD	Swin Transformer [48]	Swin-T	No	0.475	14.6
	SEST*	Swin-T	No	0.486	21.2
Event	ASTMNet [37]	Rec-Conv-SSD	Yes	0.291	21.3
Event	Spiking Swin Transformer*	Swin QKFormer	Yes	0.353	28.9
	HDI-Former*	Swin-T + Swin QKFormer	Yes	0.501	47.6
RGB + Event	SODFormer [35]	Deformable DETR	Yes	0.504	39.7
	HDI-Former	Swin-T + Swin QKFormer	Yes	0.516	47.9

set to 1. Remarkably, considering that there are only two kinds of semantic relations between tokens in the object detection task: belonging or not belonging to the same object, the RSE here is supposed to be symmetric. Therefore, only the upper triangular part is fed into the MLP to ensure symmetry, which can be summarized as:

$$S_{ij} = \begin{cases} W_m(W'_m a_{ij} + B'_m) + B_m, & i \leq j \\ S_{ji}, & i > j \end{cases}$$
 (25)

D. More Details on Experimental Setting

D.1. Gen1 Dataset

The Gen1 dataset is captured using a PROPHESEE GEN1 sensor with a resolution of 304×240 pixels. It consists of 2358 sequences, each containing recordings of open roads and various driving scenes for 60 seconds, encompassing urban environments, highways, suburban areas, and picturesque countryside landscapes. The object labels were meticulously assigned through a manual process and are available for two classes present: pedestrians and cars. The number of bounding boxes for pedestrians and cars is 228k and 27k, respectively.

D.2. More Implementation Details

Here we elaborate on some implementation details that are not covered in the Sec. 4.1. First, the spiking neuron adopted in our HDI-Former is LIFNode. In all our experiments, the reset value of LIF neurons V_{reset} is set to 0, and the membrane time constant τ to 2. We set the threshold V_{th} for the neurons following the output of self-attention to 0.5 and the rest to 1. The surrogate function engaged is the inverse trigonometric function (i.e., arctan function). The scalars attached to RPE, RSE, and dynamic interaction shown in Eq. 1-5 (i.e., λ_i , i=1,2,3,4) are set to $\lambda_1=\lambda_2=1,\lambda_3=0.3,\lambda_4=0.2$, which are decided by the experiments in Sec. E.2. Owning to a trade-off between speed and accuracy, we simply use the attention kernel function described in Eq. 3 as \mathcal{F} in Sec. 3.1. Since QKA

Table 10. The influence of the scalars (i.e. λ_1 - λ_4) involved in self-attention on the DSEC-Detection dataset [16].

$\overline{\lambda_1}$	λ_2	λ_3	λ_4	mAP	mAP ₅₀
		0.3	0.2	0.291	0.522
	1	0.3	0.5	0.286	0.514
		0.5	0.2	0.289	0.518

is equivalent to SSA with a diagonal attentional weight matrix, it benefits little from dynamic interaction. Therefore, the layers we conduct dynamic interaction start at Stage 3 in Fig. 2. We use a learning rate scheduler that decreases the learning rate by 0.1 at epochs 27 and 33.

E. More Experiments

E.1. Object Detection on PKU-DAVIS-SOD Dataset

To verify the effectiveness and generality of our HDI-Former, we further conduct an extensive experiment on the PKU-DAVIS-SOD dataset [35]. As Table 9 shows, our HDI-Former consistently outperforms the state-of-theart methods and the baselines* on the PKU-DAVIS-SOD dataset. Note that the mAP₅₀ improvement of 1.2% compared to SODFormer [35] is even more significant than the 0.9% improvement on the DSEC-Detection dataset. We attribute this to that the PKU-DAVIS-SOD dataset contains more challenging scenarios, and our HDI-Former shows a better ability to extract valid information from degraded modality with the help of dynamic interaction. We further present some instances under challenging scenarios (i.e., low light and high-speed motion blur) in Fig. 9 to verify the effectiveness of integrating events and frames and the dynamic interaction mechanism in HDI-Former.

E.2. More Ablation Studies

Influence of Scalars for RPE and RSE. To explore the influence of the hyperparameters in self-attention (i.e., λ_1 - λ_4) and choose the best hyperparameter setting, we compare the performance of HDI-Former with varying λ_i settings in Table 10. Particularly, we first follow the setting in [48] to

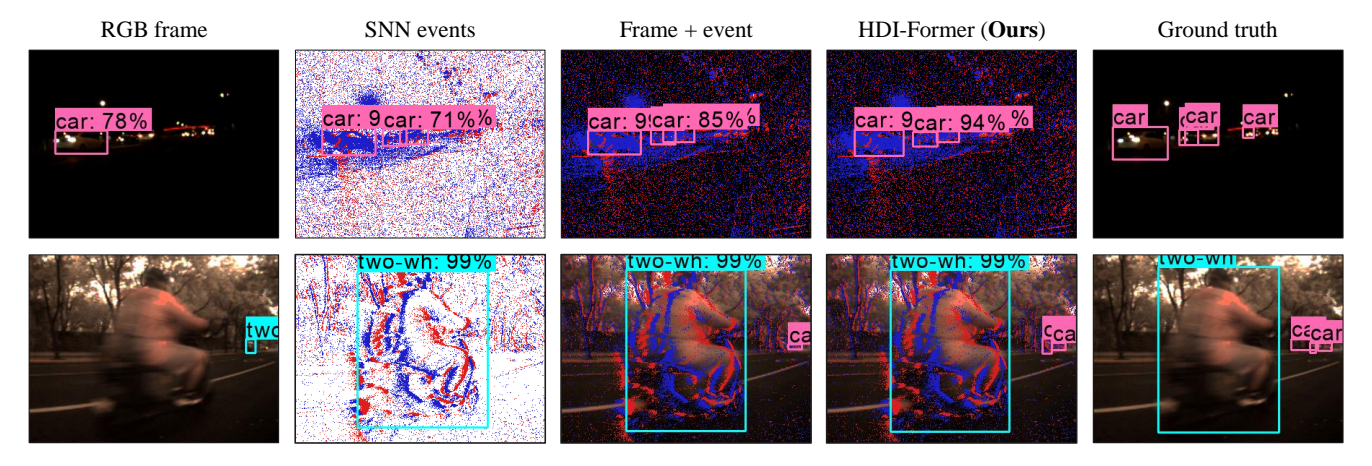


Figure 9. Representative examples demonstrate that our HDI-Former effectively detects objects by integrating events and frames in challenging scenarios on the PKU-DAVIS-SOD dataset [35].

Table 11. The influence of different attention kernel functions in dynamic interaction on the DSEC-Detection dataset [16].

Method	mAP	mAP ₅₀	Runtime (ms)
Baseline	0.291	0.522	50.3
Conv2D	0.294	0.529	61.0
MLP	0.294	0.531	73.7

set λ_1 and λ_2 to 1. For λ_3 and λ_4 which are involved in the dynamic interaction mechanism, we modify their settings to identify the best choice. From Table 10, we can observe that the performance is sub-optimal when $\lambda_4 > \lambda_3$. Moreover, the comparison between the first and the third rows in Table 10 indicates that the performance is not especially sensitive to λ_3 . Statistically, we conclude that relatively small λ_3 and λ_4 are sufficient to achieve our objective of crossmodality information interaction.

Influence of Attention Kernel Functions. The core of the dynamic interaction mechanism lies in the fact that the sharing of attention weights across modalities contributes to feature extraction. To achieve this, the attention kernel function (see Sec. 3.1) works similarly to the kernel function, projecting the attention weight of one modality into the attention weight space of the other modality since different modalities may have different attention weight spaces regarding head dimension as the channel. Akin to the kernel function, our attention kernel function is a set of functions. To explore the influence of attention kernel functions on the dynamic interaction mechanism, we compare the Baseline in Eq. 3 with more sophisticated functions like Conv2D or MLP in Table 11. As we can see, the HDI-Former achieves better performance with more powerful attention kernel functions. However, we state that the mAP improvements are marginal (i.e., 0.3%) while increasing inference time. Therefore, our implementation in Eq. 3 reaches a good trade-off between performance and complexity.

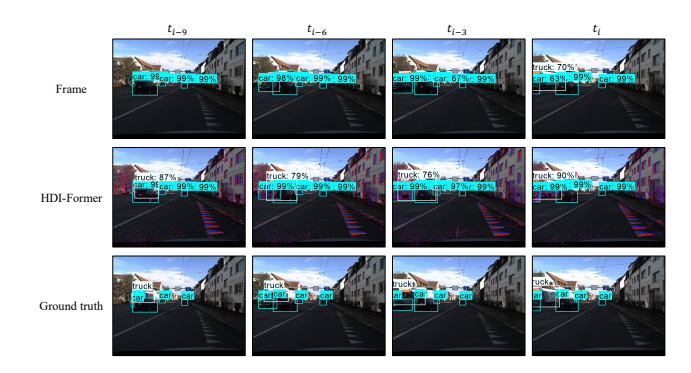


Figure 10. Representative visualization results in continuous sequences on the DSEC-Detection dataset [16]. The three rows are the frame-based SEST, our HDI-Former, and the ground truth.

E.3. More Scalability Tests

Temporal Representation Analysis Since event streams contain rich temporal cues, HDI-Former is capable of utilizing the temporal cues to boost detection performance. To validate this, we conduct additional experiments on the DSEC-Detection dataset and provide some comparative visualization results of the HDI-Former and the feed-forward baseline (i.e., SEST) about whether they utilize rich temporal cues or not (see Fig. 10). Obviously, The baseline that utilizes single RGB frames for feed-forward object detection encounters challenges in scenarios involving occluded objects, as illustrated in the first row in which the occluded truck and the second car from the left are difficult to detect. However, our proposed HDI-Former effectively addresses this challenge by harnessing rich temporal information from continuous event streams, and thus successfully detects both objects with high confidence. Moreover, in contrast to existing models that utilize temporal cues, our approach generates temporal representation by processing event streams using SNN, reducing energy consumption.

Table 12. Comparison of the inference time of the Baseline and the HDI-Former on the DSEC-Detection dataset [16].

Method	RSE	Events	Dynamic Interaction	Runtime(ms)
Baseline				16.2
(a)	$\sqrt{}$			24.7
(b)		\checkmark		50.2
HDI-Former	$\sqrt{}$	$\sqrt{}$	\checkmark	50.3

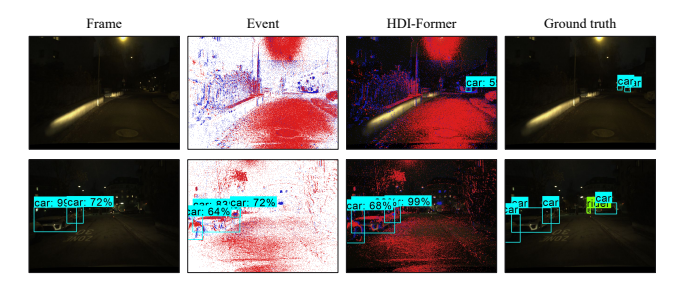


Figure 11. Representative failure cases of our HDI-Former on the DSEC-Detection dataset [16].

Inference Time Analysis Following the same experimental setup as in Sec. 4.1, we tested the inference time of the baselines and our model on an NVIDIA A100 GPU. Unfortunately, the computation architecture of most existing computing hardware is not designed for SNN, and the A100 GPU is no exception. On one hand, the inference speed of SNN on such hardware is vastly reduced; on another hand, the two branches of our HDI-Former can be executed simultaneously, while the two branches can only be executed sequentially under the existing resources, which further reduces the inference frequency. Since our HDI-Former merely increases addition operations taking advantage of SNN and few multiplications, it is without doubt that the inference speed of our HDI-Former will increase significantly on neuromorphic computation hardware.

Failure Case Analysis While our HDI-Former demonstrates promising performance even under challenging conditions, certain failure cases remain unresolved. In fact, some scenarios cannot be fully covered by the complementary properties of frames and events. This stems from the limited dynamic range of conventional frame-based cameras, resulting in poor image quality in such extreme lighting conditions. Conversely, event cameras excel at capturing moving objects but hardly output events for static or slow-motion objects. Therefore, some scenes pose a detection challenge to the current object detection paradigm, such as static objects or small objects in extreme lighting conditions. As illustrated in Fig. 11, the four columns from left to right represent two unimodal baselines, our HDI-Former, and ground truth, respectively. The first row displays the difficulty of detection in the presence of small objects under low light even with our HDI-Former. In the second row, our HDI-Former fails to figure out the static car under low light on the right. Addressing these challenges remains an important area for future research, as they extend beyond the capabilities of our HDI-Former model.